SUPPLEMENTARY INFORMATION

Biomanufactured High-Performance Triboelectric Fibers for Respirators

Khushank Singhal[1], Ramiz Boy[1], Abu Musa Abdullah[1], Tarek Mazeed[1,2], Melik C. Demirel[1,2,3,*]

[1] Department of Engineering Science and Mechanics, The Pennsylvania State University, University Park, Pennsylvania 16802, USA

[2] Huck Institutes of Life Sciences and [3] Materials Research Institute, The Pennsylvania State University, University Park, Pennsylvania 16802, USA

*Corresponding Author, E-mail: Melik@psu.edu

Number of figures: 9

Number of tables: 2

Scanning Electron Microscopy (SEM) microscopy in Figure S1 provides us with enhanced views of these two materials at 1% and 5% protein content, allowing for closer inspection of the different compositions each contains. Examining fibers with varying protein content reveals a homogenous cross-section in their micrographs for cellulose fibers compared to triacetate counterparts.

SEM micrographs in Figure S2 reveal similarities between cellulose fibers with and without protein content. At 10% protein, the morphology of as-spun fibers lacks any voids, which shows enhanced interaction between the cellulose and the proteins.

The difference in the diameters of the two fiber types is due to differences in dope solid contents and spinning parameters. The diffusion kinetics of DMSO is faster than the ionic liquid[1]. This results in the coagulation of the fiber surface faster than the fiber core. Since cellulose tends to absorb water and become plasticized, drawing resulted in a smoother surface for cellulose than triacetate. A smooth surface undergoes specular reflection, enhancing the aesthetics of the fiber. Compared to the compact structure of cellulose fibers, triacetate fibers contained nano-pores. It has been noted that the high diffusion rate of DMSO creates porous fibrils. The rapid escape of solvent from the fiber leads to faster coagulation of the dope, such that the in-line tension cannot stretch the protofibril adequately to induce a dense microstructure. Moreover, SEM micrographs of fiber cross-sections do not show phase separation of the protein. No protein precipitates in the coagulation bath were seen either.

Fourier Transform Infrared Spectroscopy (FTIR) analysis of cellulose triacetate and cellulose fibers and related solvents in Figure S3 was conducted to investigate chemical composition. The findings show that the fibers lack any solvent used in the wet-spinning of the fibers and confirm the existence of protein in the fibers.

Figure S4 shows the schematic of the triboelectric nanogenerator in both single electrode (a) and dual-electrode configurations (b). By combining protein film with two electrodes, a triboelectric nanogenerator is constructed that utilizes mechanical energy to generate electricity.

In Figure S5, cellulosic fibers coated with our proteins have been assessed as potential devices for triboelectric energy harvesting. Our analysis revealed that their output can reach an impressive maximum when configured in either single or two-electrode systems, potentially opening new avenues of exploration in energy harvesting. Both open circuit voltages (VOC) and short-circuiting currents (ISC) were tracked to assess performance levels across the context range studied here.

Figure S6 shows a schematic, which offers an insight into how the materials employed in this study interact electrostatically, as illustrated by their respective positions on the triboelectric series.

Protein deposits have been observed to coat the surfaces of cellulose fibers, in Figure S7, when viewed under a SEM micrograph, providing an interesting insight into uniform structure on this scale.

Figure S8 shows distinct views from cross-section as well as lateral surface visuals. These SEM micrographs revealed that wood cellulose fibers can be drawn into finer diameter of 15 microns. While mechanisms including impaction, diffusion, and interception are responsible for most of the filtration efficiency of respirators (83 – 92%)[2], extending the efficiency further by engineering the filter architecture alone is futile. This restriction is overcome by introducing surface charges on constituent fibers, allowing particulate capture by the electrostatic mechanism. N95 respirators, commonly based on polypropylene electret, portray filtration efficiencies of over 95%[3,4]. However, the standard methods of charging fibers, i.e., induction and corona discharge, require hundreds of kilovolts, making the processes extraordinarily energy-intensive and hazardous[5]. The industry can realize the triboelectric effect through carding[6].

Several recent studies report on the triboelectric effect in filtration systems. While some utilize triboelectric nanogenerator devices as powering systems, others employ the fibrous media directly as respirators[7,8]. Das *et al.* fabricated a wool-based nonwoven media using conventional textile technologies and achieved over 60% reduction in penetration on average[6]. He *et al*. have reported a triboelectric respirator designed to control humidity within, with a filtration efficiency of 98.83%[9]. And others demonstrate a respirator with a dedicated self-charging design to prolong effectiveness[8,10]. Moreover, triboelectric filtration systems and respirators have been introduced in markets, as reported by Liu *et al*[7]. These commercial products perform at par with conventional filtration systems like N95 masks and High-Efficiency Particulate Air (HEPA) filters. Biobased membranes exhibit high filtration efficiencies as well[11]. Furthermore, as shown in the studies, biopolymer fibers can be triboelectrically charged in a facile manner to further their performance. Herein, by incorporating unique bioengineered SRT protein, the triboelectric performance of cellulosic fibers was enhanced significantly. Since the filtration efficiency of filters is directly correlated to the surface charge density of fibers[12], the functionalization of fibers by proteins is highly favorable. Moreover, by modifying the amount of protein in the blend, the triboelectric properties of the fibers can be fine-tuned. Yim *et al.* studied three N95 and four KN95 commercial respirators. While the surface charge density on KN95 was lower, their filtration efficiency was comparable to that of NIOSH-approved N95 masks[2,4]. Therefore, if the filter architecture is optimized appropriately per the mechanical mechanisms, it can portray high performance even with low surface charge density. The general construction of a respirator comprises an outer protective, filter (middle), and inner protective polymeric fibrous layers. While the filter layer is the main functional element, the protective layer provides structural support and safety. Cellulose esters are promising substitutes for polymers for protective coatings. They are desirable from the viewpoints of their mechanical properties and high hydrophobic nature[13]. Being hydrophobic, the cellulosic layers would keep moisture from the filter layer, preventing extensive charge decay in humid conditions. Moreover, with the lowering of fiber diameter, the filtration efficiency of the filter improves exponentially[14]. We demonstrate the versatility of the wet spinning process by spinning finer and more delicate cellulose-protein fibers. High molecular weight cellulose was spun into filaments of diameter ~ 15 μm (**Fig. S8**), approximately one-half of the cellulose blend

fibers. Finer fibers also exhibit more substantial triboelectric charge generation due to higher specific surface area.

We performed protein-leaching on cellulose (10% protein) fibers using DMSO as a proof of concept for recyclability. Initially, fibers were kept in an oven at 60 °C for one hr. to remove moisture. 215 mg of filaments were immersed in 50 ml of DMSO at 60 °C and were continuously stirred for a day. Following the DMSO treatment, the fibers were centrifuged to remove excess DMSO. The fibers were then washed and transferred to warm ultrapure water for 1 hr. Lastly, the fibers were dried in an oven (at 60 °C) for 3 – 4 hrs. and stored in a desiccator before characterization. Post-treatment of filaments, the protein was separated from DMSO by adding ultrapure water in excess. Recycling of fibers is essential in textiles to prolong sustainability. **Fig. S9a** shows the residue extracted from fibers. FTIR spectra (**Fig. S9b**) confirmed protein extraction from fibers. DMSO-treated fibers show reduced Amide I and II band intensities, which are also apparent in the protein residue. Recyclable synthetic proteins are desirable due to high production costs and modest yield. Upon DMSO treatment, fibers underwent significant morphological changes (see **Fig. 3c main text**). Coalescence of surface regions was seen. We posit that since cellulose swells in DMSO and water[15], the projected parts underwent coalescence during drying. However, the significant change during protein leaching was impressing porosity to fibers. The diameter of treated fibers was higher by ~ 2 μm, amounting to a net porosity of 10%. Porous cellulose fibers are excellent candidates as carbon fiber precursors, and they find applications in flexible and wearable electronics, radiative cooling textiles, aerospace, etc[16,17].

Tables S1 and S2 show the list of literature referred in the main text and surface areas of fibers used in this study, respectively. The maxima of output voltages of polymer and cellulose-based devices are similar, with the materials being ZnO-doped polyvinylidene fluoride with nylon and nitrocellulose membranes with crimped paper, respectively **(Table S1**). Moreover, several materials are often integrated to achieve considerable performance (as high as 5), including Ag nanowires, $BaTiO_3$, MXene, fluorinated polymers, silanes, carbon nanotubes, graphene oxide, and many more. We achieved performance enhancement by incorporating a single protein variant, thus, curbing material diversity. Additionally, Shen *et al.* discussed polypropylene-based devices. They used Aluminum as the positive layer. The maximum voltage attained at 10 N normal force was approx. 20 V. In addition to fabrics, they tested commercial surgical masks and N95 filter layers. The max voltages for the mask and N95 were 10 and 13 V, respectively. Compared to our biopolymer-protein fibers, the triboelectric performance of polypropylene was inferior

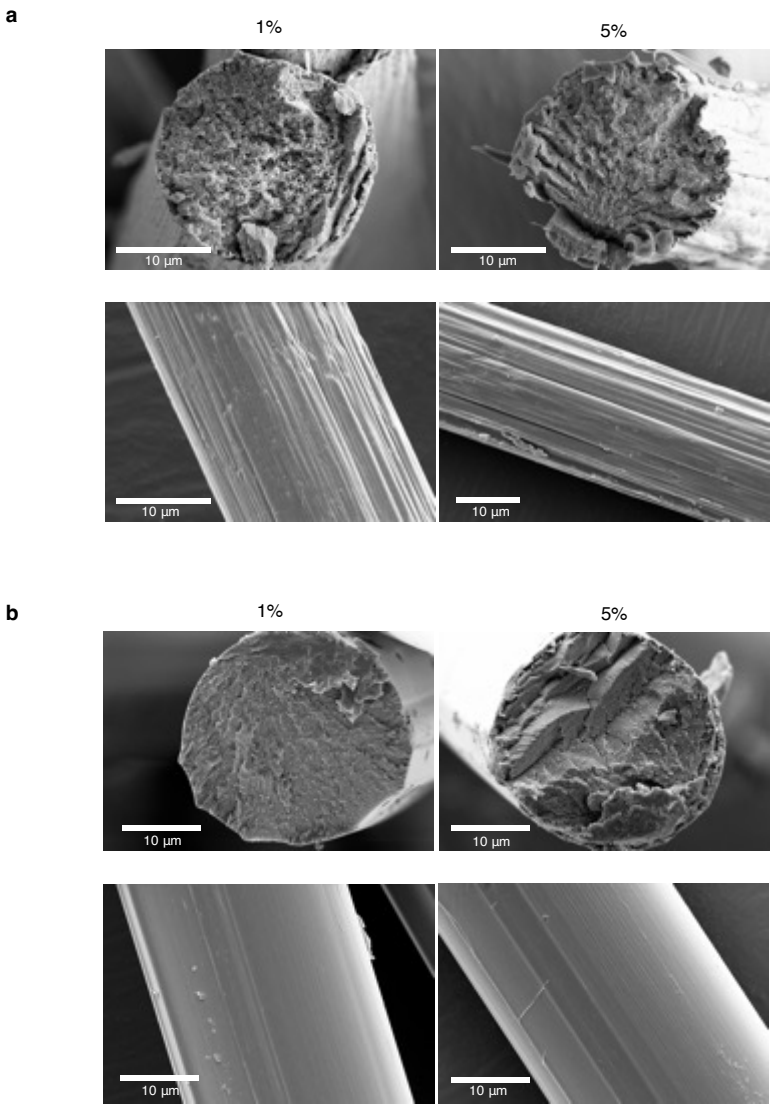

Figure S1. SEM micrographs of cellulose triacetate (**a**) and cellulose (**b**) fibers with 1% and 5% protein content. 10% is shown in the Figure 3a of the main text.

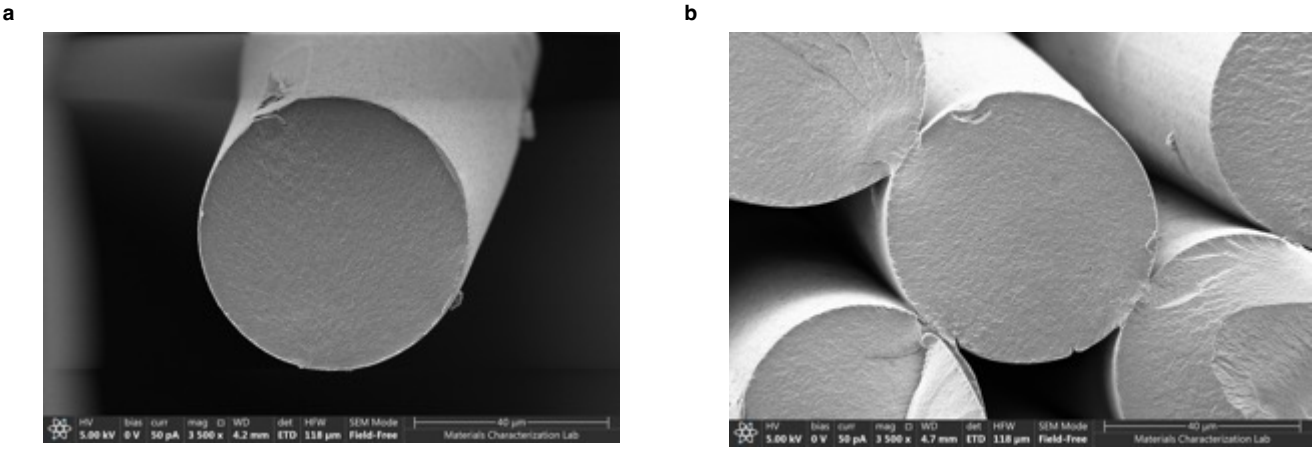

Figure S2. SEM micrographs of as-spun cellulose fibers with no protein (**a**), and 10% protein (**b**) content. As-spun fibers are collected in the coagulation bath prior to any drawing.

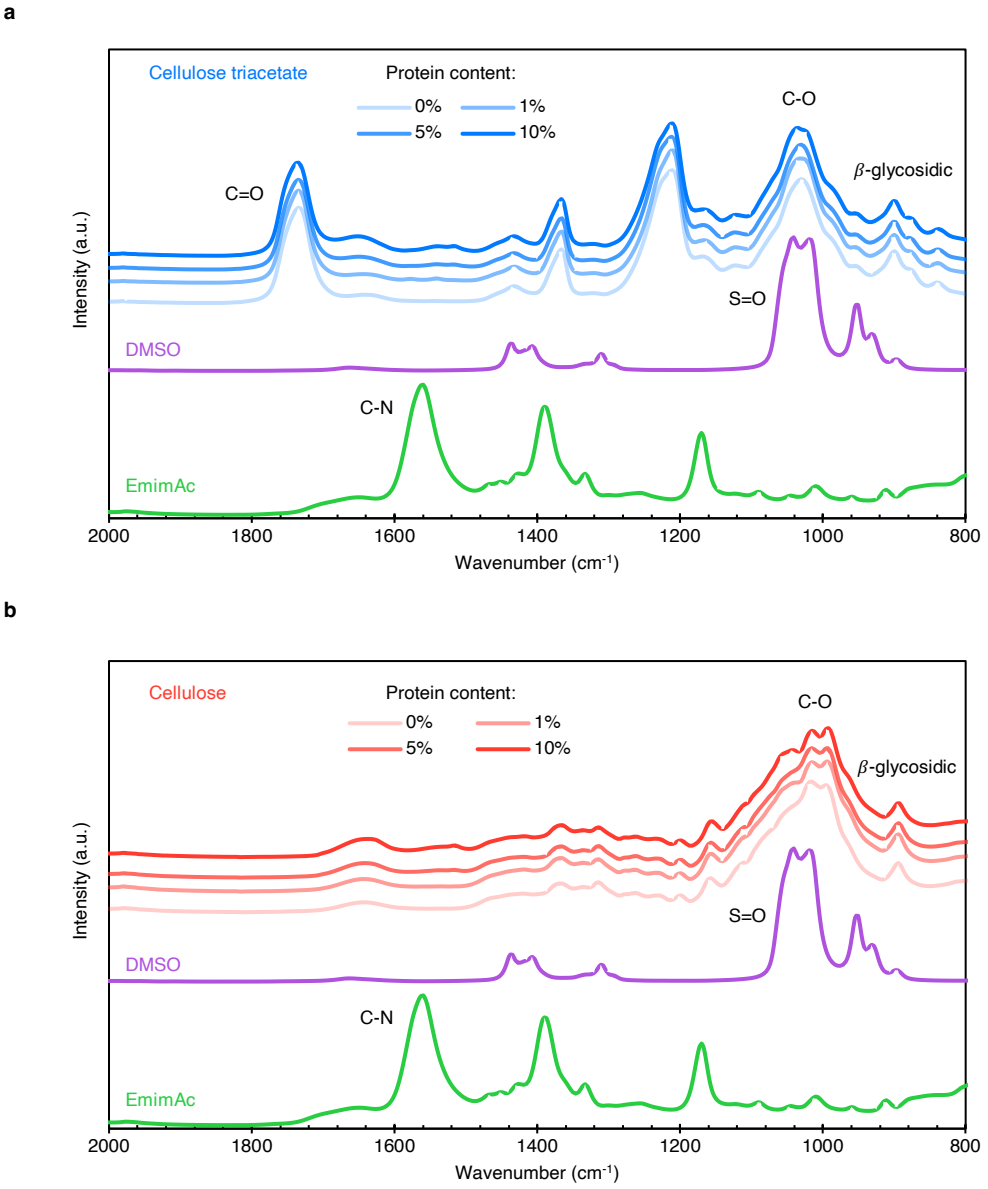

Figure S3. FTIR of cellulose triacetate (**a**) and cellulose fibers (**b**) with all protein contents are shown. The spectra of the solvents are included as well.

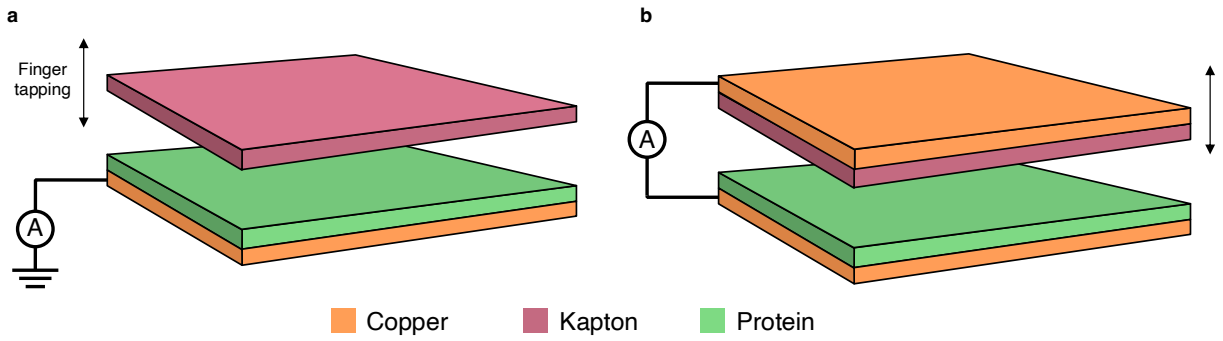

Figure S4. Illustration of the construction of the bioengineered protein film-based single electrode (**a**) and two-electrode (**b**) triboelectric nanogenerators.

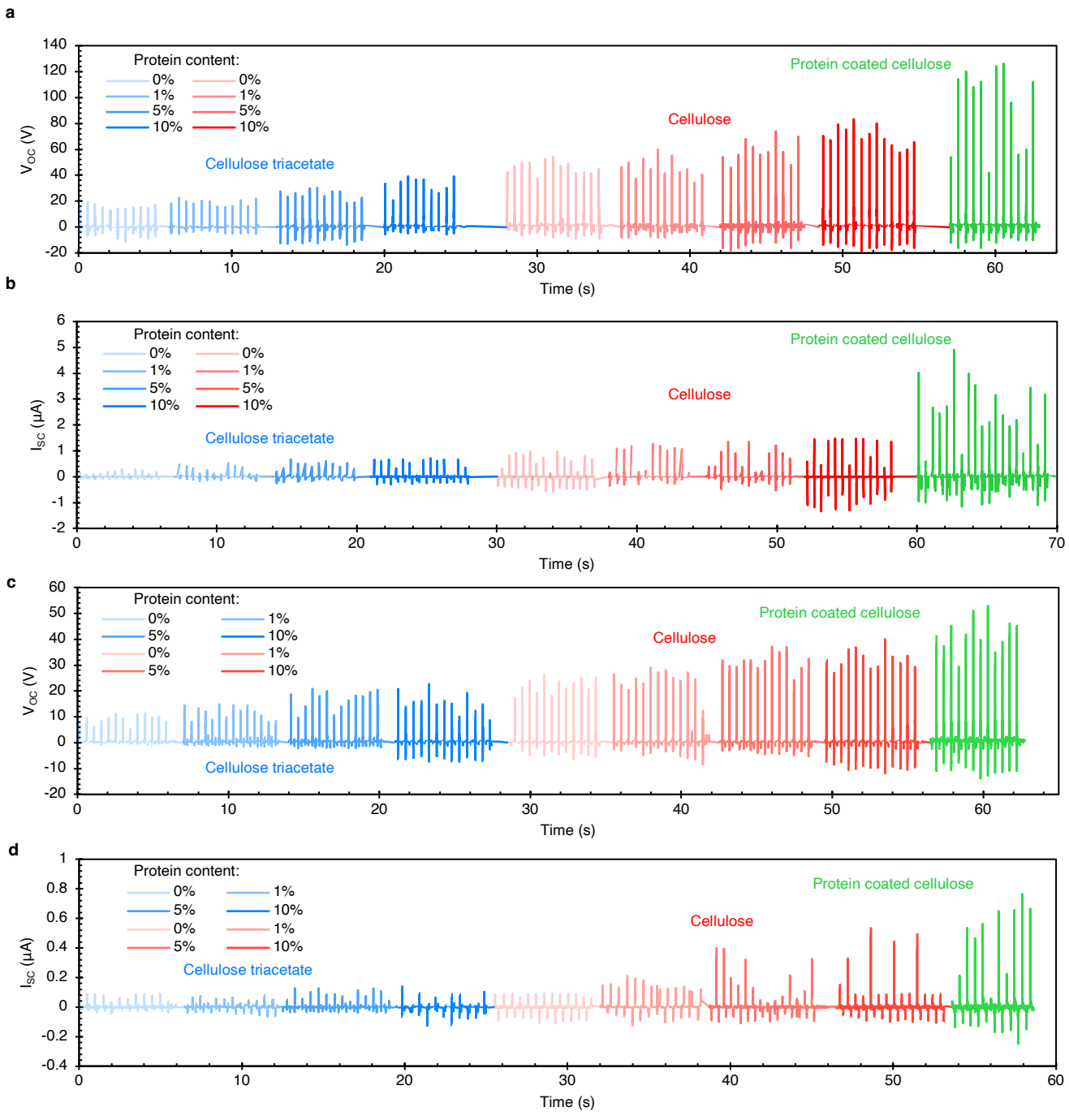

Figure S5. Triboelectric output of fiber-based devices in single (**a, b**) and two-electrode (**c, d**) configurations. V_{OC} and I_{SC} denote open-circuit voltage and short-circuit current, respectively. The results for protein-coated cellulose fibers represent maximum attainable output through blending with protein.

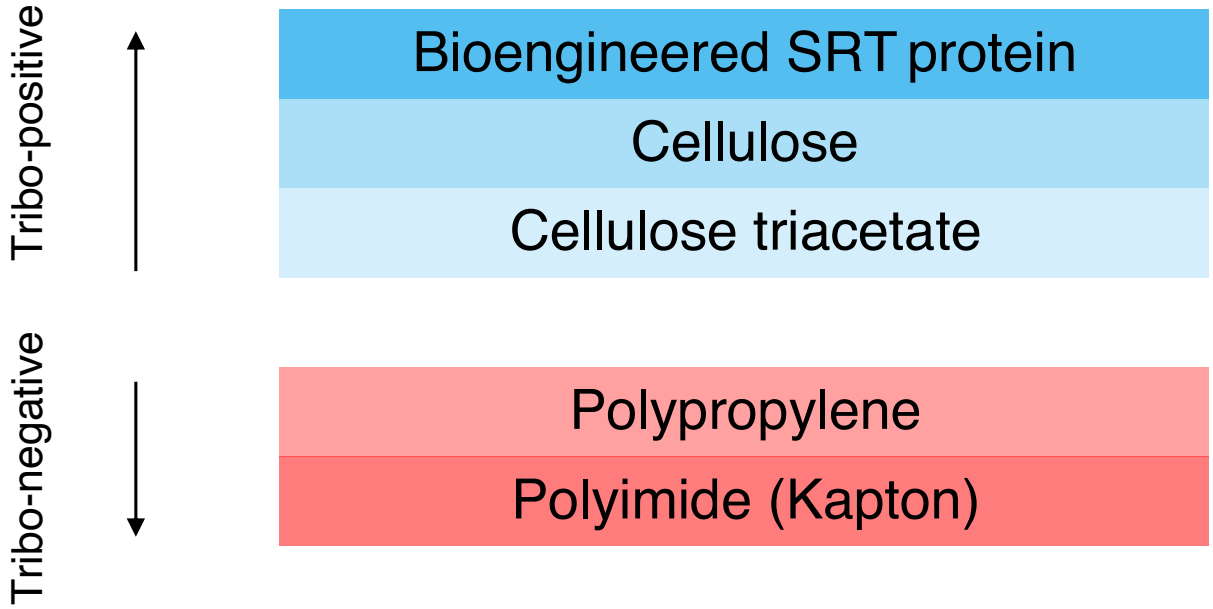

Figure S6. The schematic for the triboelectric series showing the relative positions of the materials used in this study.

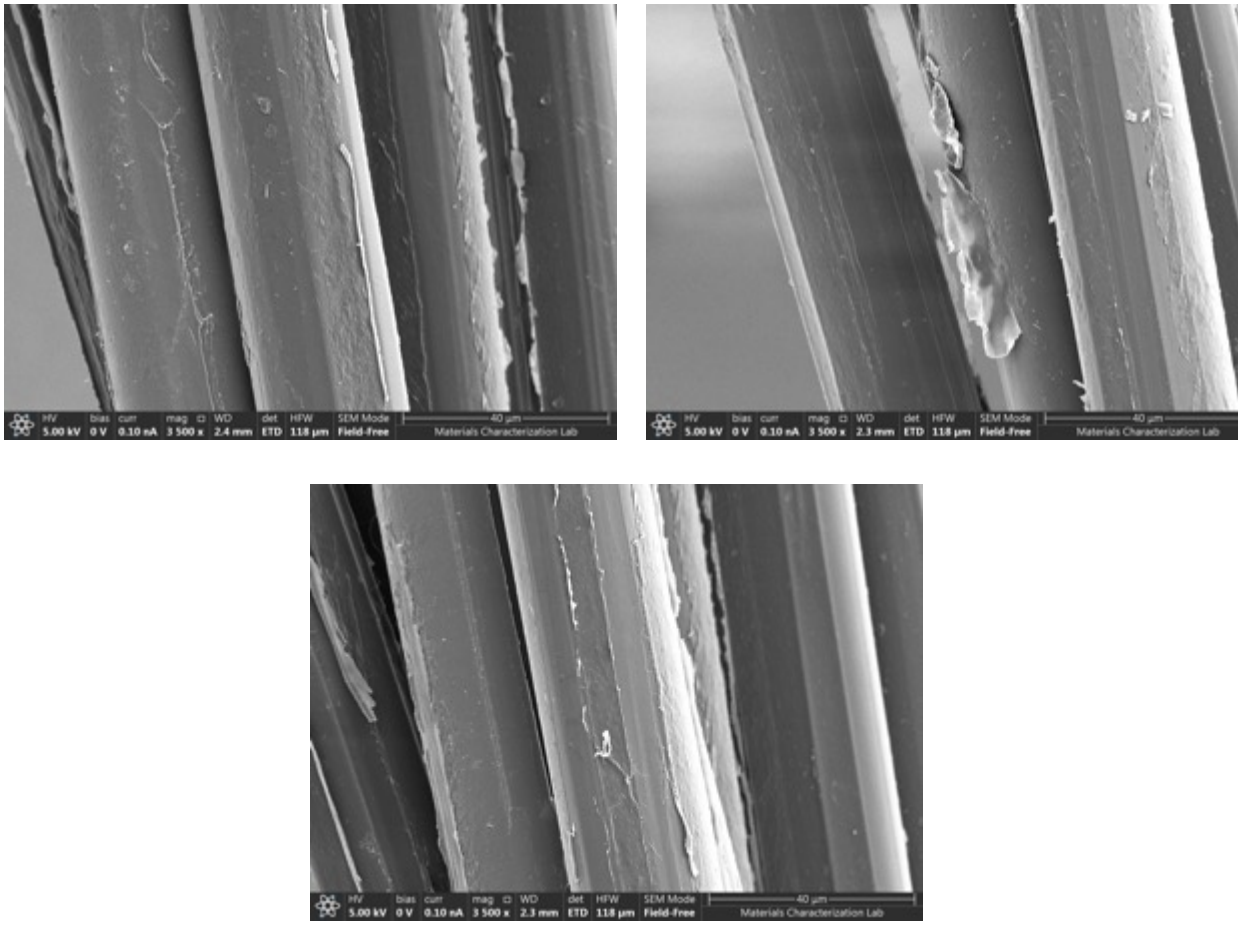

Figure S7. SEM micrographs of the protein-coated cellulose fibers. Protein deposits can be noticed on the fiber surface.

a

b

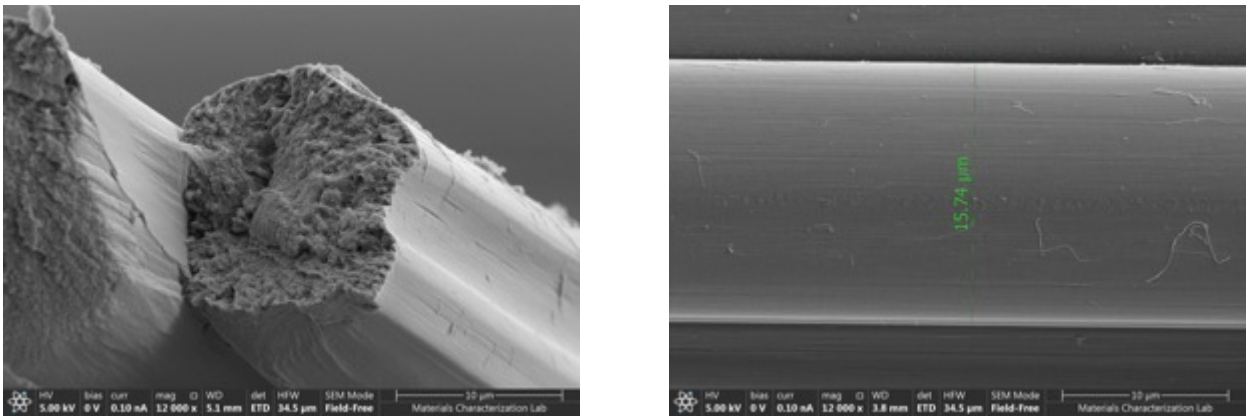

Figure S8. SEM micrographs showing the cross-section and lateral surface of wood (high molecular weight) cellulose-protein composite fibers. A diameter of ~15 µm was attained.

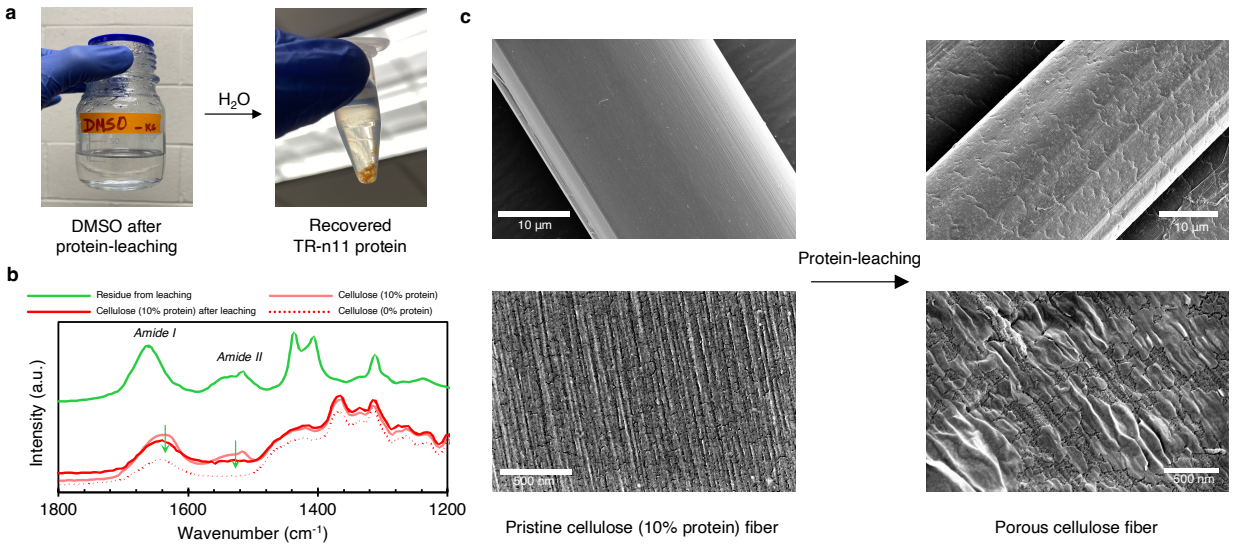

Figure S9. Protein recovery from blend fibers. **a.** The protein dissolved in DMSO, after leaching out of the fibers, can be precipitated using water. **b.** FTIR spectra of the residue from DMSO treatment and the treated fibers show protein presence and reduced protein content, resp. **c.** SEM micrographs showing the change in fiber microstructure after DMSO treatment. The diameter of the fibers increased by about 2 µm, indicating increased porosity.

Table S1. The list of literature referred in **Figure 5**.

Category	S. No.	Reference	Materials*
Polymer based	1.	D Shen *et al.* ACS Appl. Mater. Interfaces 2021, 13, 34266 – 34273.	PP, Al, Cu, N95 filter, surgical mask
	2.	HJ Oh *et al.* Polymers 2020, 12, 1044.	TPU, PP, Ni-coated fabric
	3.	N Cui *et al.* ACS Appl. Mater. Interfaces 2015, 7 18225 – 18230.	PA6, Cu, cotton, dacron
	4.	SSH Abir *et al.* ACS Appl. Mater. Interfaces 2021, 13, 60401 – 60412.	PLA, Cu, TPU/Au, PVDF
	5.	M Zhou *et al.* Nano Energy 2016, 27, 439 – 446.	PTFE, PA6, Graphene
	6.	H Li *et al.* Adv. Mater. Technol. 2018, 3, 1800065.	PTFE, PA6, Ag
	7.	K Dong *et al.* ACS Nano 2017, 11, 9490 – 9499.	SS/PET, Si-rubber
	8.	X Pu *et al.* Adv. Mater. 2015, 27, 2472 – 2478.	PET, Ni, parylene
	9.	SS Kwak *et al.* ACS Nano 2017, 11, 10733 – 10741.	PTFE, Ag
	10.	S Jung *et al.* Adv. Mater. 2014, 26, 6329 – 6334.	PI, PU, PDMS, Al, carbon fabric
	11.	Q Qiu *et al.* Nano Energy 2019, 58, 750 – 758.	PET, PVDF NFs, PTFE NPs, CFab
	12.	Z Tian *et al.* Nano Energy 2017, 39, 562 – 570.	PET, Si-rubber, Ni
	13.	YE Shin *et al.* J. Mater. Chem. A 2018, 6, 22879.	Al, PA6, PVDF, CFab,
	14.	T Zhou *et al.* ACS Appl. Mater. Interfaces 2014, 6, 14695 – 14701.	PA6, PET, Ag

	15.	MF Lin *et al.* Nano Energy 2018, 44, 248 – 255.	PDMS, PVDF-HFP, Cu, Kapton
	16.	A Yu *et al.* ACS Nano 2017, 11, 12764 – 12771.	PU, SS, PET
	17.	T He *et al.* Nano Energy 2019, 57, 338 – 352.	Si-rubber, PEDOT:PSS, Al, PTFE
	18.	R Cao *et al.* Nano Research 2018, 11(7), 3771 – 3779.	AgNPs, PVDF, PET, PAN, TPU
	19.	Z Lin *et al.* Adv. Funct. Mater. 2018, 28, 1704112.	CFab, PET
	20.	J Song *et al.* Materials 2018, 11, 2120.	Ag, chinlon, PDMS, SS
	21.	YH Ko *et al.* RSC Adv. 2015, 5, 6437.	Ni/PET, PDMS-CFab
	22.	T Kim *et al.* Nano Energy 2018, 54, 209 – 217.	PA6, PTFE, Au, PU
	23.	X Hou *et al.* ACS Appl. Mater. Interfaces 2018, 10, 43661 – 43668.	Si, PET, CFab
	24.	S Lee *et al.* Nano Energy 2015, 12, 410 – 418.	PDMS, Al NP coated fabric
	25.	YC Lai *et al.* Adv. Funct. Mater. 2017, 27, 1604462.	Si, SS, skin (as electrode)
	26.	W Yang *et al.* Adv. Mater. Technol. 2019, 4, 1900745.	PVA/H_3PO_4, CNT/WPU,
	27.	S Bairagi et al. ACS Appl. Mater. Interfaces 2022, https://doi.org/10.1021/acsami.2c13092	PET, PVDF, PA6, silk, Al
	28.	X Pu et al. Chemical Engineering Journal 2020, 398, 125526.	PVDF, PA6, ZnO, Al
Protein based	29.	K Yan *et al.* J. Mater. Chem. A 2020, 8, 22745.	CMCS, CMC-Na, Au
	30.	AY Choi *et al.* Scientific Reports 2017, 7, 45583.	Silk, Si-rubber, CFab

	31.	R Cao *et al.* ACS Nano 2018, 12, 5190 – 5196.	Si, PA6, CNT, skin (as electrode)
	32.	SB Jeon *et al.* Nano Energy 2018, 53, 596 – 603.	Cotton, Ni, wool, skin (as electrode)
	33.	W Wang *et al.* Nano Energy 2020, 71, 104605.	Si, Cu, liquid metal, PTFE
	34.	T Charoonsuk et al. Nano Energy 2021, 89, 106430.	Chitosan, silk, PTFE, Al
	35.	C Ye *et al.* Nano-Micro Lett. 2020, 12:12	Silk, SS, PTFE
	36.	Z Li *et al.* Nano Energy 2018, 53, 726 – 733.	PS, PES, CA, Cu, PMMA, PI
	37.	J Huang *et al.* ACS Appl. Mater. Interfaces 2021, 13, 24774 – 24784.	EC/PA6, PVDF/MXene, Cu
	38.	X He *et al.* Adv. Funct. Mater. 2018, 28, 1805540.	CEL, CNF, Ag, FEP
	39.	W Yang *et al.* Adv. Mater. Technol. 2018, 3, 1800178.	Paper, PVDF
	40.	I Kim *et al.* Nano Energy 2018, 53, 975 – 981.	CNF, AgNW
	41.	C Qian *et al.* Nano Energy 2019, 63, 103885.	PET, Ag, PDMS, CNF
	42.	L Zhang *et al.* Adv. Mater. Technol. 2016, 1, 1600147.	Cotton, CFab, PA6
	43.	X He *et al.* Nano Energy 2017, 39, 328 – 336.	Paper, ITO, PDMS/PVDF, FEP
Cellulose based	44.	H Oh *et al.* Adv. Funct. Mater. 2019, 29, 1904066.	AgNW, $BaTiO_3$, bacterial-CEL, PTFE, Al
	45.	L Gu *et al.* ACS Appl. Mater. 2021, 13, 5133 – 5141.	Paper, nitro-CEL, Cu

46.	XS Zhang *et al.* Nano Energy 2017, 33, 393 – 401.	Paper, PTFE, graphite
47.	T Huang *et al.* Nano Energy 2019, 58, 375 – 383.	Cotton, PTFE, CFab, PET
48.	S Chen *et al.* Nano Energy 2019, 61, 69 – 77.	Cu, paper, nitro-CEL
49.	C Yao *et al.* Nano Energy 2016, 30, 103 – 108.	FEP, ITO, PET, CNF
50.	S Parandeh *et al.* Nano Energy 2019, 59, 412 – 421.	Paper, PCL/GO, Au
51.	X Shi *et al.* ACS Sustainable Chem. Eng. 2019, 7, 18657 – 18666.	CEL, nitro-CEL, pyrrole-CEL
52.	X Pu *et al.* Adv. Mater. 2016, 28, 98 – 105.	Cotton, PET, Ni, parylene
53.	S Hao *et al.* Nano Energy 2020, 75, 104957.	Wood, PTFE, Cu
54.	Y Feng *et al.* J. Mater. Chem. A 2016, 4, 18022.	Al, paper, PET, PVDF, Ag, PI
55.	B Chen *et al.* Nano Energy 2018, 44, 468 – 475.	Acrylic, PET, ITO, FEP, CNC
56.	C Yao *et al.* Adv. Funct. Mater. 2017, 27, 1700794.	CNF, methyl-CNF, nitro-CNF, FEP-CNF, Cu
57.	J Wang et al. Sustainable Energy Fuels 2022, 6, 1974 – 1982.	Cu, PTFE, lignin
58.	A Rajabi-Abhari et al. ACS Appl. Mater. Interfaces 2021, 13, 219 – 232.	CEL, CNF, PTFE, Al
59.	J Xiong *et al.* Adv. Energy Mater. 2017, 7, 1701243.	MCC, HCOENPs, PET, Au, CFab

*Ag: silver, Al: aluminum, Au: gold, CA: cellulose acetate, CEL: cellulose, CFab: conductive fabric, CMC-Na: carboxymethyl cellulose sodium, CMCS: carboxymethyl chitosan, CNC: cellulose nanocrystals, CNF: cellulose nanofibril, CNT: carbon nanotube, Cu: copper, EC:

ethyl cellulose, FEP: fluorinated ethylene propylene, GO: graphene oxide, HCOENPs: hydrophobic cellulose oleoyl ester nanoparticles, HFP: Poly(vinylidene fluoride-co-hexafluoropropylene), ITO: indium tin oxide, Ni: Nickel, NF: nanofiber, NP: nanoparticle, NW: nanowire, PA6: Nylon, PAN: polyacrylonitrile, PCL: polycaprolactone, PDMS: polydimethylsiloxane, PEO: polyethylene oxide, PES: polyethersulfone, PET: polyester, PI: polyimide, PLA: polylactic acid, PMMA: polymethylmethacrylate, PP: polypropylene, PS: polystyrene, PTA: terephthalic acid, PTFE: polytetrafluoroethylene, PU: polyurethane, PVA: polyvinyl alcohol, PVDF: Polyvinylidene fluoride, SF: silk fibroin, Si: silicon, SS: stainless steel, TPU: thermoplastic polyurethane.

Table S2. Effective surface areas (in cm^2) of fiber-based devices.

Fiber type	**Device type**	**Protein content (%)**			
		0	**1**	**5**	**10**
Cellulose triacetate	Single electrode	1.92	2.19	2.17	2.28
	Two electrodes	2.19	2.20	1.90	2.03
Cellulose	Single electrode	2.13	2.28	2.15	2.07
	Two electrodes	2.09	2.26	2.29	2.11
Protein-coated cellulose	Single electrode	2.05			
	Two electrodes	2.08			

References

1. Lee, Y. J. *et al.* Structure and Mechanical Properties of Regenerated Cellulose Fibers Wet-Spun from Ionic Liquid/Cosolvent Systems. *Fibers Polym.* **20**, 501–511 (2019).
2. Yim, W. *et al.* KN95 and N95 Respirators Retain Filtration Efficiency despite a Loss of Dipole Charge during Decontamination. *ACS Appl. Mater. Interfaces* **12**, 54473–54480 (2020).
3. Rengasamy, S., King, W. P., Eimer, B. C. & Shaffer, R. E. Filtration Performance of NIOSH-Approved N95 and P100 Filtering Facepiece Respirators Against 4 to 30 Nanometer-Size Nanoparticles. *J. Occup. Environ. Hyg.* **5**, 556–564 (2008).
4. Electronic Code of Federal Regulations. Title 42: Public Health, Part 84: Approval of Respiratory Protective Devices. (2020).
5. Tsai, P. P., Schreuder-Gibson, H. & Gibson, P. Different electrostatic methods for making electret filters. *J. Electrost.* **54**, 333–341 (2002).
6. Das, D. & Waychal, A. On the triboelectrically charged nonwoven electrets for air filtration. *J. Electrost.* **83**, 73–77 (2016).
7. Liu, J., Jiang, T., Li, X. & Wang, Z. L. Triboelectric filtering for air purification. *Nanotechnology* **30**, 292001 (2019).
8. Peng, Z. *et al.* Self-charging electrostatic face masks leveraging triboelectrification for prolonged air filtration. *Nat. Commun.* **13**, 7835 (2022).
9. He, X. *et al.* A Hierarchically Nanostructured Cellulose Fiber-Based Triboelectric Nanogenerator for Self-Powered Healthcare Products. *Adv. Funct. Mater.* **28**, 1805540 (2018).
10. Liu, G. *et al.* Self-Powered Electrostatic Adsorption Face Mask Based on a Triboelectric Nanogenerator. *ACS Appl. Mater. Interfaces* **10**, 7126–7133 (2018).

11. Deng, Y. *et al.* Bio-based electrospun nanofiber as building blocks for a novel eco-friendly air filtration membrane: A review. *Sep. Purif. Technol.* **277**, 119623 (2021).
12. Thakur, R., Das, D. & Das, A. Electret Air Filters. *Sep. Purif. Rev.* **42**, 87–129 (2013).
13. Ioelovich, M. Adjustment of Hydrophobic Properties of Cellulose Materials. *Polymers* **13**, 1241 (2021).
14. Payen, J. *et al.* Influence of fiber diameter, fiber combinations and solid volume fraction on air filtration properties in nonwovens. *Text. Res. J.* **82**, 1948–1959 (2012).
15. Cuissinat, C., Navard, P. & Heinze, T. Swelling and dissolution of cellulose. Part IV: Free floating cotton and wood fibres in ionic liquids. *Carbohydr. Polym.* **72**, 590–596 (2008).
16. Zhou, Z., Liu, T., Khan, A. U. & Liu, G. Block copolymer–based porous carbon fibers. *Sci. Adv.* **5**, eaau6852 (2019).
17. Peng, Y. *et al.* Nanoporous polyethylene microfibres for large-scale radiative cooling fabric. *Nat. Sustain.* **1**, 105–112 (2018).